Two-Dimensional Electronic Double-Quantum Coherence Spectroscopy

JEONGHO KIM,[†] SHAUL MUKAMEL,[‡] AND
GREGORY D. SCHOLES[*,†]

†Department of Chemistry, Institute for Optical Sciences and Centre for Quantum Information and Quantum Control, University of Toronto, 80 St. George Street, Toronto, Ontario M5S 3H6, Canada, ‡Department of Chemistry, University of California, Irvine, California 92697

CONSPECTUS

The theory of electronic structure of many-electron systems, such as molecules, is extraordinarily complicated. A consideration of how electron density is distributed on average in the average field of the other electrons in the system, that is, mean field theory, is very instructive. However, quantitatively describing chemical bonds, reactions, and spectroscopy requires consideration of the way that electrons avoid each other while moving; this is called electron correlation (or in physics, the many-body problem for fermions). Although great progress has been made in theory, there is a need for incisive experimental tests for large molecular systems in the condensed phase.

In this Account, we report a two-dimensional (2D) optical coherent spectroscopy that correlates the double-excited electronic states to constituent single-excited states. The technique, termed 2D double-quantum coherence spectroscopy (2D-DQCS), uses multiple, time-ordered ultrashort coherent optical pulses to create double- and single-quantum coherences over time intervals between the pulses. The resulting 2D electronic spectrum is a map of the energy correlation between the first excited state and two-photon allowed double-quantum states. The underlying principle of the experiment is that when the energy of the double-quantum state, viewed in simple models as a double HOMO-to-LUMO (highest occupied to lowest unoccupied molecular orbital) excitation, equals twice that of a single excitation, then no signal is radiated. However, electron−electron interactions, a combination of exchange interactions and electron correlation, in real systems generates a signal that reveals precisely how the energy of the double-quantum resonance differs from twice the single-quantum resonance. The energy shift measured in this experiment reveals how the second excitation is perturbed by both the presence of the first excitation and the way that the other electrons in the system have responded to the presence of that first excitation.

We compare a series of organic dye molecules and find that the energy offset for adding a second electronic excitation to the system relative to the first excitation is on the order of tens of millielectronvolts; it also depends quite sensitively on molecular geometry. These results demonstrate the effectiveness of 2D-DQCS for elucidating quantitative information about electron−electron interactions, many-electron wave functions, and electron correlation in electronic excited states and excitons.

Our work helps illuminate the implications of electron correlation on chemical systems. In a broad sense, we are trying to help address the fundamental question "How do we go beyond the orbital representation of electrons in the chemical sciences?"
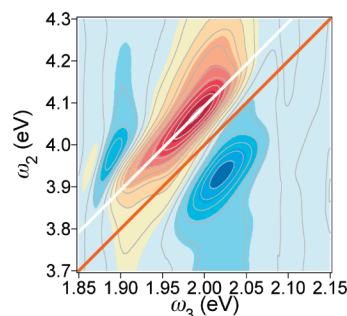
1. Introduction

Recent advances in theory and practice of multidimensional coherent spectroscopy have enabled researchers to go beyond ultrafast measurements of excited state dynamics and to gain deeper insights into the mechanism of excited state processes.[1−8] Coherent multidimensional optical spectroscopy has great potential for revealing molecular structural details and dynamics in complex multichromophore systems. In contrast to multidimensional nuclear magnetic resonance techniques, which probe spin−spin interactions

and can track changes with millisecond time resolution, the optical analog allows us to probe changes in couplings between multiple chromophores absorbing at visible or infrared frequencies with femtosecond time resolution. Here we report the experimental demonstration of a new two-dimensional (2D) electronic coherent spectroscopy that maps electronic states in such a way that insight can be gained into the electronic structure of excited states, in particular how electron correlations change upon photoexcitation.

The technique, termed 2D double-quantum coherence spectroscopy (2D-DQCS), uses multiple, time-ordered ultrashort laser pulses to induce coherences between ground, single-excited, and double-excited electronic states.[9−12] The Fourier evaluation of a third-order signal scanned along two coherence time intervals between the pulses produces a 2D spectrum that maps out the energies of and correlations among excited electronic states that are excited via one- and two-field interactions from the electronic ground state. The measured 2D-DQC spectrum provides unique information on the electronic structure of double-quantum resonances with respect to constituent single-quantum states. Conceptually related experiments involving double-quantum coherence were already implemented at NMR radio[13] and infrared frequencies[12] to provide effective probes of interactions among spins and anharmonicity of molecular vibrations, respectively. When applied to study electronic excitations in molecules, 2D-DQCS can be naturally interpreted in terms of electronic oscillations (quasiparticles) as is common in other many-body fermion systems in the condensed phase, such as semiconductors. In weakly interacting electron systems, like many inorganic semiconductors, the electron correlation effects are directly measured by this experiment.[9,10] Experimental studies of semiconductors using this method have been reported.[14,15] Thus, 2D-DQCS can unify the description of electronic excitations in complex molecular and nanoscale systems.

Here we study molecular chromophores, where the interactions among electrons and their correlations are well-known to be substantial. For example, exchange interactions, as seen in singlet−triplet splitting, are on the order of 0.5 eV, compared with a few millielectronvolts and smaller for inorganic nanocrystals and bulk semiconductors.[16] Furthermore, the electron correlation energy, comparable to chemical bonding energies, is essential for determining molecular geometries and for the prediction of excited state wave functions and energies with chemical accuracy.[17−21] We envision that a contribution of this experiment will be to provide an experimental benchmark for the most challenging quantum-chemical
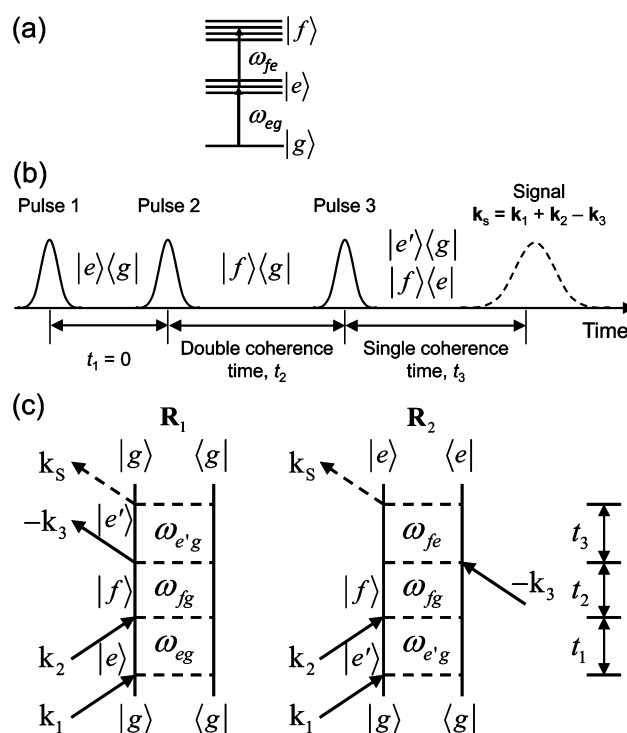

FIGURE 1. (a) A three-level system consisting of ground (*g*) and manifolds of single (*e*) and double (*f*) excited states. (b) A sequence of three coherent pulses inducing the 2D-DQC signal. (c) The two Feynman diagrams contributing to the 2D-DQC signal.

calculations, those of high-lying electronic excited states with substantial double-excitation character.[22,23]

The goal of this Account is to show that 2D-DQCS data can be recorded for large molecules in the condensed phase and the signals are consistent with predictions from theory. We thereby show that many-electron systems may be readily investigated. Effects captured by mean-field theories together with correlation corrections ultimately contribute to the data. There are still unresolved challenges for obtaining and interpreting the data. Perhaps the most demanding challenge for future work is to elucidate more deeply how to communicate the implications of electron correlation on chemical systems. In other words, how do we go beyond the orbital representation of electrons in chemical sciences? The ability to quantify electron correlation by experiment will stimulate interest in that question.

2. Theory and Simulations of 2D-DQCS

Two-dimensional DQCS uses a sequence of three coherent optical pulses to correlate certain electronic coherences in a three-level system consisting of ground state (*g*), a manifold of single excited states (*e*), and a manifold of double excited states (*f*), as shown in Figure 1a. The time ordering of a sequence of three femtosecond laser pulses applied to this
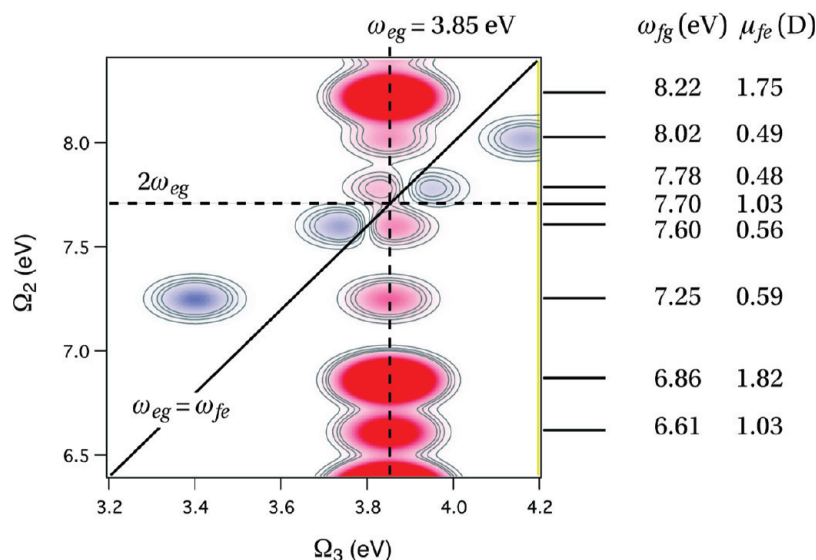
FIGURE 2. Example of a 2D-DQC spectrum calculated for a model system. See text for details.

system is shown in Figure 1b. Pulse 1 interacts with the system to create a coherence between g and e. A coherence is a quantum superposition represented by an off-diagonal element of the density matrix, in this case $\rho_{eg} = |e\rangle\langle g|$. After a time delay, t_1, pulse 2 interacts with the system to create an electronic coherence between g and f, that is, the double-quantum coherence. For simplicity, t_1 is set to be zero such that the first two pulses create the double-quantum coherence via two-field interactions. After a double coherence time delay, t_2, the system interacts with pulse 3, which induces either a single-quantum coherence between g and e' or a coherence between f and e. During a time period, t_3, termed "single coherence time", the third-order polarization, $P^{(3)}$, is radiated in the direction of $\mathbf{k}_s = \mathbf{k}_1 + \mathbf{k}_2 - \mathbf{k}_3$, where $\mathbf{k}_1$, $\mathbf{k}_2$, and $\mathbf{k}_3$ are wave vectors of pulse 1, 2, and 3, respectively. The induced third-order polarization, $P^{(3)}(t_2,t_3)$, is measured by scanning the time delays t_2 and t_3. Then, 2D Fourier transformation of $P^{(3)}(t_2,t_3)$ with respect to t_2 and t_3 delivers 2D spectra as a function of two frequency axes, ω_2 and ω_3, which are conjugates to t_2 and t_3, respectively. It should be noted that, instead of scanning the t_3 time delay, its conjugate frequency, ω_3, is directly obtained using a combination of spectrograph and CCD array detector. Since one frequency axis is already obtained by a dispersed detection scheme, only the Fourier transformation along the t_2 delay is needed to produce an (ω_2, ω_3) 2D spectrum:

$$S_{2D}(\omega_2, \omega_3) = \int_{-\infty}^{\infty} iP^{(3)}(t_2, \omega_3) \exp(i\omega_2 t_2)\, dt_2 \quad (1)$$

The two quantum pathways contributing to the induced third-order signal can be represented by the Feynman diagrams, displayed in Figure 2c. Each diagram shows the sequence of field−matter interactions and the evolution of the electron density matrix of the system during the time intervals between each interaction. The 2D-DQC signal, $S(\omega_3, \omega_2)$, is given by[10]

$$S(\omega_2, \omega_3) = \sum_{e,e'f} (\omega_2 - \omega_{fg})^{-1}[\mu_{ge}\mu_{ef}\mu_{fe'}\mu_{e'g}(\omega_3 - \omega_{e'g})^{-1} -$$

$$\mu_{ge'}\mu_{e'f}\mu_{ge}\mu_{fe}(\omega_3 - \omega_{fe})^{-1}] \quad (2)$$

The two terms in the brackets are the contributions of the pathways $\mathbf{R}_1$ and $\mathbf{R}_2$. Both share the common term $(\omega_2 - \omega_{fg})^{-1}$, and thus the energies of double-quantum resonances, ω_{fg}, are projected along the ω_2 axis. In contrast, along the ω_3 axis, $\mathbf{R}_1$ and $\mathbf{R}_2$ contribute differently to the signal, which results in their interference. The first pathway gives the energies of single-quantum resonances between ground and single excited states, that is, $\omega_3 = \omega_{e'g}$. The second reveals resonances between double and single excited states, $\omega_3 = \omega_{fe}$. Thus, 2D-DQCS correlates the energies of double-quantum resonances, ω_{fg}, to those of single-quantum resonances, $\omega_{e'g}$ and ω_{fe} in a 2D spectrum.

To orient the reader, an example of a 2D-DQCS map over a broad energy range for the molecule dibenz[a,h]anthracene calculated according to eq 2 is shown in Figure 2. The electronic states and the dipole strength for transitions among them were calculated using the SAC-CI/6-31G method. According to this method (note that the results are highly method-dependent because the quantum-chemical approach is approximate), there are 41 electronic states lying below 9 eV. Of these, eight can be optically excited from the lowest energy singlet excited state, and they are listed on the right side of the figure. Red peaks are contributed by $\mathbf{R}_1$ and blue

troughs (negative peaks) come from R_2. The blue and red peaks are displaced symmetrically along the ω_3-axis about the diagonal $\omega_{fe} = \omega_{eg}$. These features map out the energies of the $|f\rangle$ states relative to $|e\rangle$. Certain of the $|f\rangle$ states contain significant contributions ($\sim$30%) from determinants that represent double excitation from the HOMO to LUMO. It is these states that reveal information about electron correlation, as discussed below.

It has been predicted that the two pathways R_1 and R_2 interfere in a unique manner to make 2D-DQCS powerful for directly probing the signatures of electron correlation effects.[10,24] For independent electrons, where the correlations between electrons are totally absent, the double excited state, f, is given by a direct product of the single excited states, e and e'. In this case, $\omega_{e'g} = \omega_{fe}$, and, owing to exact cancellation of the two signal contributions in the bracket, the 2D-DQC signal vanishes. An example of where this model can be useful is a semiconductor, where e is the exciton and f is the biexciton. However, when quantum confinement effects are significant, say in quantum dots, the exciton acquires a notable fine structure (owing mainly to exchange interactions),[25−27] and that alone ensures $\omega_{e'g} \neq \omega_{fe}$ even in a mean-field approach.[28]

Molecules are even more challenging to understand. First, the exchange interaction (singlet−triplet splitting) is significant,[29] and this raises the energy of the first singlet excited state ω_{eg} relative to $\omega_{fg}/2$ by a few hundred millielectronvolts. Therefore, at zeroth-order, the data recorded by 2D-DQCS is captured by mean-field theoretical approaches. Second, there is substantial differential electron correlation between the three primary states, g, e, and f, probed in the experiment. Usually f is lowered even more relative to e. In some systems, like polyenes, f can even lie below e.[22,30,31] Third, it is essential to go beyond a two-electron, four-orbital description of the system because there are prominent single-excitation configurations with energies $\sim 2\omega_{eg}$ and appropriate symmetries. Such configurations are already known to be very important for determining third-order nonlinear susceptibilities.[32,33]

An important difference between our experimental results and the theoretical results previously reported[10,23] (cf. Figure 2) is that femtosecond laser pulses limit spectral bandwidth (130−150 meV fwhm), and therefore we only measure specific correlations between the first electronic excited state and the f state(s) at close to double this excitation energy, as permitted by the bandwidth. Finite pulse duration effects can be included according to the modified form of eq 2 that includes the frequency-domain pulse envelopes.[34] Model quantum-
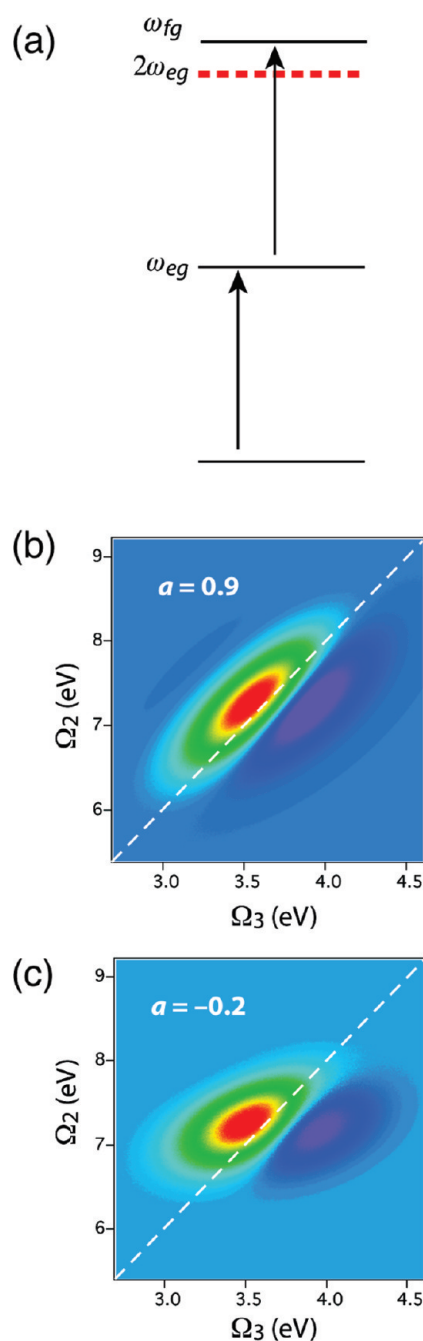

FIGURE 3. (a) The three-level collective electronic oscillator model. (b, c) Simulated 2D-DQC spectra of the three-level system for different values of the correlation strength, a, between the fluctuations $\delta\omega_{eg}$ and $\delta\omega_{fe}$.

chemical calculations (Figure 2) indicate that outside this energy bandwidth there can be features of significantly greater intensity.

We have modeled a simple three-level system, Figure 3, with the f state up-shifted relative to e, consistent with our experimental results. In the simulations, the generally weaker negative peak relative to the observed strong positive peak has been empirically accounted for using a scaling factor of

0.75. We have assumed Gaussian homogeneous line shapes. Transition energy gap fluctuations were incorporated by introducing the fluctuations, $\delta\omega_{ij}$, via energy offsets sampled from a Gaussian distribution using a Monte Carlo procedure, for example, $\omega'_{eg} = \omega_{eg} + \delta\omega_{eg}$. At each iteration, two random offsets are selected: δ_1 and δ_2. The transition energies are then given by $\delta\omega_{eg} = \delta_1$, $\delta\omega_{fe} = a\delta_1 + (1 - |a|)\delta_2$, and $\delta\omega_{fg} = \delta\omega_{eg} + \delta\omega_{fe}$, where a marks the extent to which the fluctuations $\delta\omega_{eg}$ and $\delta\omega_{fe}$ are correlated. If $a = 0$, then the fluctuations are uncorrelated, which would be the case for two independent particle excitations. More generally, a can vary between $a = 1$ (entirely correlated) and $a = -1$ (anticorrelated). Simulations displayed in Figure 3 show that the strongly correlated case ($a \approx 1$), which yields the marked signal elongation parallel to the diagonal, is most consistent with the experimental results reported below.

3. Data Acquisition and Evaluation

The details of the laser setup are described elsewhere.[35] Briefly, optical pulses with 130 fs pulse duration and 800 μJ of pulse energy were generated at 775 nm from a 1 kHz repetition rate Ti:sapphire amplified laser (Clark-MXR, CPA-2001). They were converted into visible light tunable from 450 to 650 nm by a noncollinear optical parametric amplifier (NOPA). The NOPA output pulses were sent to a pair of quartz prisms for precompensation for material dispersion. The laser pulses were characterized at the sample position by transient grating frequency-resolved optical gating (TG-FROG) of pure solvent (ethanol). Near-transform-limited pulses were obtained with a pulse duration of 18−22 fs at the sample position, depending on the wavelength, and a time−bandwidth product of ∼0.47. The compressed NOPA output was split by a beamsplitter, and these two beams were focused and spatially overlapped on a diffractive optic with a 25 cm focal length lens to give a pair of replicas at ±1 diffraction orders for each beam. This provided phase-locked pulse pairs $E_1 - E_{LO}$ and $E_2 - E_3$. Phase-stable time delays between the pulses with suboptical period precision is required to perform Fourier transforms without artifacts. Such precise control of time delays was achieved by using pairs of movable glass wedges inserted into E_1, E_2, and E_3 beams, as was introduced by Fleming and co-workers for 2D electronic photon echo spectroscopy.[7] The double coherence time, t_2, was scanned by simultaneously moving both pulse 1 and 2, while the time delay, t_4, between the pulse 3 and LO remained constant. To ensure sufficient sampling of the double-quantum resonance frequencies, the t_2 scan was made in 0.1 fs time steps, giving the Nyquist fre-
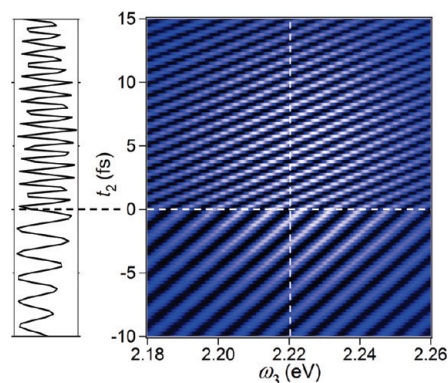

FIGURE 4. Measured 2D-DQCS raw data of phenoxazone 9 plotted in terms of t_2 vs ω_3 axes. A series of interferograms along the ω_3 axis were recorded on the CCD detector as a function of t_2 delay.

quency of four times the double-quantum resonance frequencies of the measured samples. The rest of the setup, measurement, and data analysis is more-or-less standard for 2D electronic spectroscopy and will be documented in detail elsewhere.

A notable feature of our approach is that we use the usual phase-locked pulse pairs generated by the diffractive optic (DO), rather than requiring fully phase-locked pulses. The reason that this works successfully for the DQCS experiment is that we use a scan sequence isomorphic to that used in "normal" 2D photon echo spectroscopy, where the signal arrives in the $\mathbf{k}_{PE} = -\mathbf{k}_1 + \mathbf{k}_2 + \mathbf{k}_3$ direction and the pulse pairs E_1/E_2 and E_3/E_{LO} are inherently phase-locked. In this case, the phase of the DO-based setup is stabilized because fluctuations in phase of the four pulses prior to the DO cancel out between phase-locked pulse pairs, that is, $(\varphi_2 - \varphi_1) + (\varphi_3 - \varphi_{LO}) = 0$. For the DQCS experiment, we use the same four-beam configuration,[36] but we relabel $E_1 \leftrightarrow E_3$. In this case, the signal is radiated in the new direction of $\mathbf{k}_{DQC} = \mathbf{k}_1 + \mathbf{k}_2 - \mathbf{k}_3$ and the E_3/E_2 and E_1/E_{LO} pulse pairs are locked in phase. The phase stability is still maintained consistently with the phase matching condition of the DQC signal by simply relabeling the pulses 1 and 3, that is, $(\varphi_2 - \varphi_3) + (\varphi_1 - \varphi_{LO}) = 0$. Therefore, the inherent phase stability achieved by the DO-based setup also applies to the 2D-DQCS experiment.

In the 2D-DQCS, a double-quantum coherence is created between ground state and double excited states due to the interactions of the system with the first two pulses. To clearly demonstrate the DQC feature and its contrast to a single-quantum coherence, raw 2D data obtained from the scan of the time delay t_2 at both positive and negative values are shown in Figure 4. To keep the t_4 delay constant for the success of heterodyne detection using spectral interferometry, the time delay t_2 was scanned by moving both pulses 1 and 2 at $t_2 \geq$

0, as described above, while moving only pulse 3 at $t_2 < 0$. When $t_2 > 0$, the pulses 1 and 2 first interact with the sample, creating the double-quantum coherence between the ground (g) and double excited (f) states. As the system in the double-quantum coherence evolves over t_2, the radiated third-order signal oscillates at a frequency of ω_{fg}. In contrast, when $t_2 < 0$, pulse 3 arrives first to create the single-quantum coherence between the ground (g) and single excited (e) states. Accordingly, the signal oscillates at a single-quantum coherence frequency, ω_{eg}, which is about half of ω_{fg}. Such contrast in signal oscillation frequencies at positive and negative t_2 values highlights the major difference of two 2D optical coherent spectroscopies: 2D photon echo spectroscopy (2D-PES) vs 2D-DQCS. The oscillation arising from single-quantum coherence observed in the negative t_2 range yields the 2D-PE signal.[6,7] Only double-quantum-coherence oscillations measured at positive t_2 values are relevant to 2D-DQCS, where the correlations between double-quantum resonance and single-quantum resonance energies are mapped out in a 2D spectrum. In other words, the signals measured at positive and negative t_2 values are of different origin, and all the data used for processing the 2D spectra presented in this Account are collected at only $t_2 \geq 0$.

The 2D-DQC spectra are complex quantities that have both amplitude and phase. In this Account, we present the real part (Re) and absolute value (Abs) of the spectra; the former represents the absorptive contribution of the third-order polarization, while the latter includes both absorption and refractive index contributions. For phasing of the 2D-DQC spectra, we invoke the projection-slice identity,[6,37] which relates the (absorptive) real part of the projection of the 2D-DQC spectrum onto the ω_3 axis and separately measurable spectrally resolved pump−probe signal measured at $t_2 = 0$. The comparison of the projection of a 2D spectrum with the spectrally resolved pump−probe signal was already employed in the phasing strategies in the 2D-PES.[6,37] Here, it should be noted that although the 2D-DQC signal is radiated in a direction ($\mathbf{k}_s = \mathbf{k}_1 + \mathbf{k}_2 - \mathbf{k}_3$) that is different from that of the pump−probe signal ($\mathbf{k}_{PP} = \pm\mathbf{k}_1 \mp \mathbf{k}_2 + \mathbf{k}_3$), these two signals become indistinguishable at $t_2 = 0$ ($t_1 \equiv 0$ in 2D-DQCS), when all three pulses are coincident in time. Why this should be the case is evident by referring to Figure 4. The absorptive contribution of the slice at $t_2 = 0$ of the "normal" 2D-PE signal (in the lower half), after divided by the spectral interference pattern using the above-described Fourier transform methods, is equivalent to the spectrally resolved pump−probe signal with zero pump−probe time delay. Since the 2D-DQC signal in the upper half shares the common $t_2 = 0$ slice with 2D-PE signal
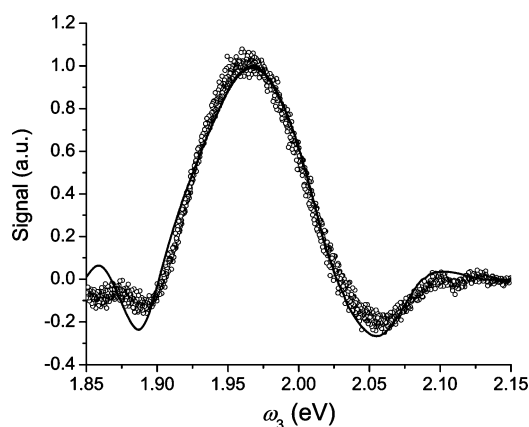

FIGURE 5. Phasing of 2D-DQC spectra of Nile blue. The projection of 2D-DQC spectrum onto the ω_3 axis (solid line) and the spectrally resolved pump−probe spectra at $t_2 = 0$ (open circles) are matched well.
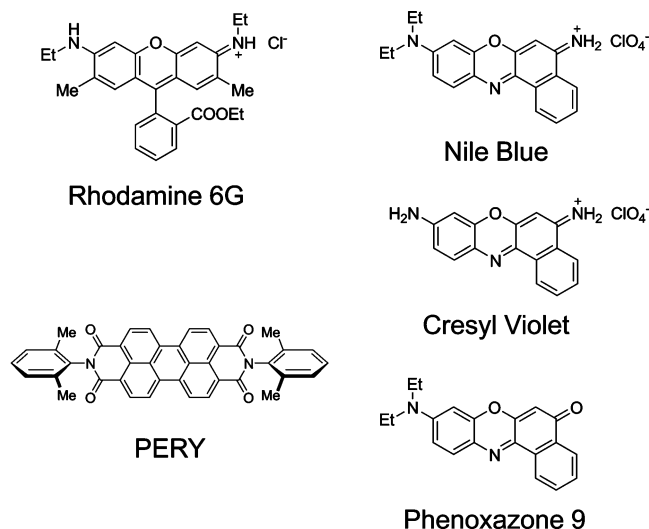

FIGURE 6. Molecular structures of organic dyes studied using the 2D-DQCS measurements.

in the lower half, the spectrally resolved pump−probe signal can be used for phasing of 2D-DQC spectra as well. Hence, the phase of the 2D-DQC spectra is adjusted so that the real part of projection of 2D spectrum onto the ω_3 axis matches the profile of the pump−probe spectrum that is separately measured at $t_2 = 0$, as shown in Figure 5.

4. Results and Discussion

The 2D-DQCS was applied to study a series of organic dyes. They include rhodamine 6G (R6G), N,N'-bis(2,6-dimethylphenyl)perylene-3,4,9,10-tetracarboxylic diimide, a derivative of perylene diimide (PERY), Nile blue (NB), cresyl violet (CV), and phenoxazone 9 (Phen9), Figure 6. The samples were purchased and used as received in solution form, dissolved in toluene (PERY) or ethanol (all other samples). The optical
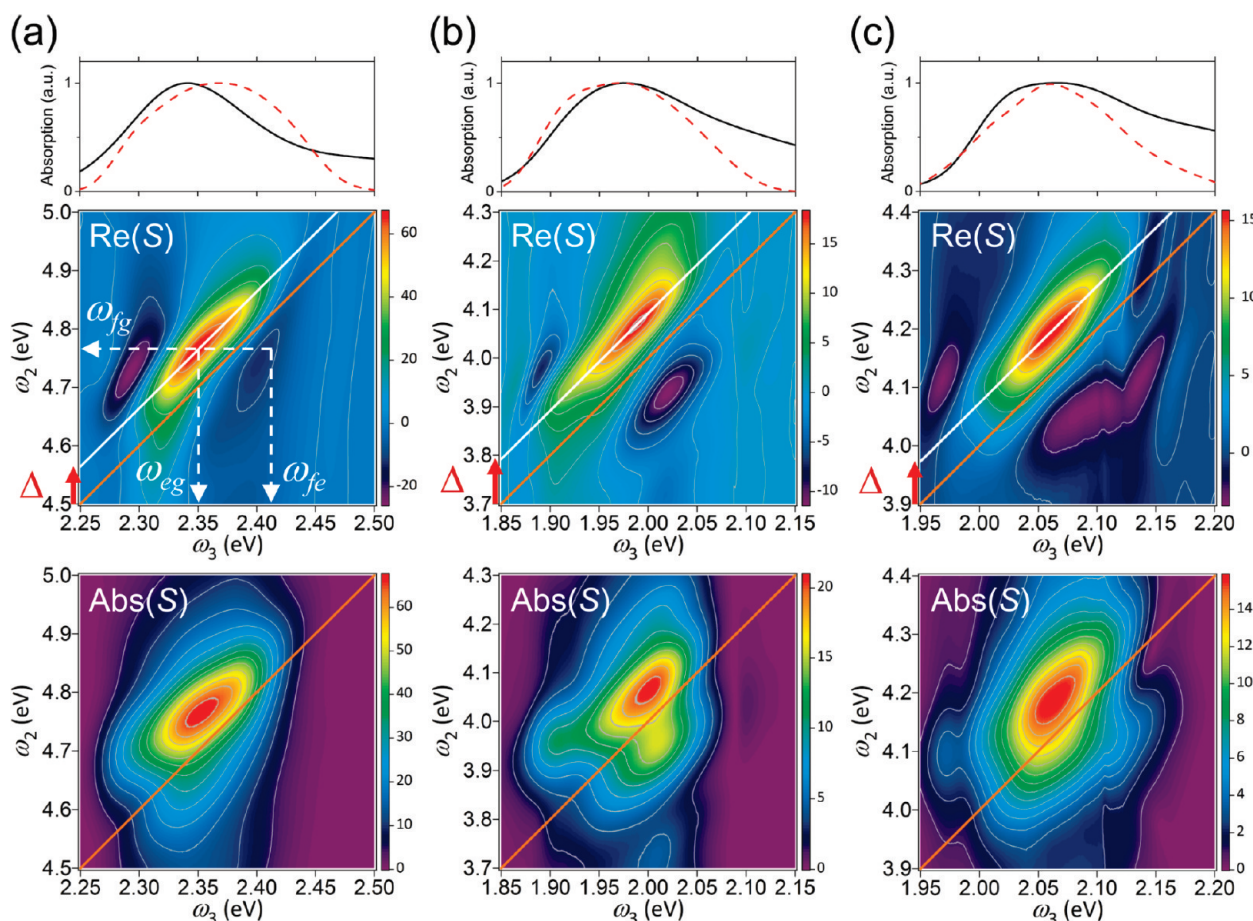
FIGURE 7. The 2D-DQC spectra of (a) rhodamine 6G, (b) Nile blue, and (c) cresyl violet. The real part, Re(S), and absolute value, Abs(S), of the complex 2D spectra are shown in the middle and lower panels, respectively. The absorption spectra (black solid line) and laser spectra (red dashed line) are shown for comparison in the upper panels. The diagonal line (orange) of $\omega_2 = 2\omega_3$ represents the double-quantum resonance energies when there is no correlation between single excitations. For the organic dyes measured in this work, Δ is 64 meV (R6G), 73 meV (PERY), 102 meV (NB), 94 meV (CV), and 89 meV (Phen9). The error range of the Δ value precision is about $\pm5\%$.

densities of samples were kept at ~0.4 in a 1 mm path length quartz cuvette.

The 2D-DQC spectra of R6G, NB, and CV are shown in Figure 7. The diagonal line, $\omega_2 = 2\omega_3$, serves as a reference for the energies of measured double-quantum states because it represents the case when $\omega_{fe} = \omega_{e'g}$ and thus $\omega_{fg} = 2\omega_{e'g}$. The Re spectrum exhibits much narrower features than the Abs spectrum, as is typical for 2D photon echo spectroscopy.[6,7] Although the Abs spectrum still exhibits an overall pattern of the peaks, it contains an averaged response of absorptive and refractive contributions, thus much more broadened peak features.

All of the Re spectra shown in Figure 7 contain two main peaks, one on the left and one to the right of the diagonal. As expected from theory,[11] these peaks have oppositely signed amplitudes. In the simulated 2D-DQC spectra shown in Figure 2, both peaks are elongated along the diagonal, while the peak width in the antidiagonal direction is narrow and well

resolved. The width of the peaks along the ω_3 axis reflects the inhomogeneous line width of the transition from the ground state to single excited state. The peak position along ω_2 axis represents the energy of the double-quantum resonance, ω_{fg}. On the other hand, the positions of the left and right peaks along the ω_3 axis reveal the energies of the relevant single-quantum resonance, ω_{eg}, and its correlation-induced shifted resonance, ω_{fe}, respectively. The positive ω_{eg} peak is stronger. The weaker negative ω_{fe} peak can be ascribed to (1) smaller oscillator strength of the $e \rightarrow f$ transition compared with that of $g \rightarrow e$ transition or (2) limited spectral bandwidth and finite temporal duration of the laser pulses used in our measurements. When the energy of the two peaks along the ω_2 axis is compared, the negative ω_{fe} peak appears at a lower energy than the positive ω_{eg} peak, more significantly in the 2D spectra of NB and CV. Such a difference in ω_2 energy between the two peaks can be also caused by the limited laser pulse

spectral bandwidth, which limits the visible width of the ω_{fe} peak in the 2D spectra.

In addition to these main features, an extra negative peak is seen on the left of the ω_{eg} peak at a slightly lower energy on the ω_2-axis in Figure 7. We do not see this feature in all data collected and believe it is most likely an artifact. We have carried out calculations that show the 2D-DQC spectra are strongly influenced by the vibronic structure in the electronic transitions, leading to the appearance of additional cross-peaks or peak distortions, adding rich structure to the 2D-DQC spectra and diminishing the intensity of the negative peak relative to the positive one. We also note that sample thickness can distort 2D line shapes compared with theoretical expectations.[38]

A line passing through the maximum of the ω_{eg} peak along the diagonal is compared with the diagonal line to obtain the energy shift of the peak relative to the diagonal. The energy offset along the ω_2 axis provides a direct signature of correlation between two single excitations comprising a double-quantum state. The double-quantum correlation energy found from the positive peak $\Delta_+ = \omega_{fg} - 2\omega_{eg}$ is shown in Figure 2a. An experimental challenge is that the ω_2-axis is critically dependent on calibration of the t_2 delay, and small uncertainties are manifest as the asymmetry of the positive and negative peaks about the diagonal. Therefore, it might be better to estimate Δ using the average $(\Delta_+ + \Delta_-)/2$, where Δ_- is determined from the position of the negative peak. Δ is central to this measurement because it quantifies the change in the energy of the double-quantum state (relative to double the single-quantum energy) induced by the interaction between the two single-quantum excitations. By analogy to vibrational oscillators,[12] Δ represents the anharmonicity of the collective electronic oscillator (quasiparticle). The Δ value is equivalent to the difference between the positions of the two peaks along the ω_3 axis, $\omega_{fe} - \omega_{e'g}$, indicating the correlation strength between the ω_{eg} and ω_{fe} transitions. In accordance with the upshift of the ω_{eg} peak from the diagonal, the Δ values of all the organic dyes examined in this work are positive. This implies that the double-quantum state is destabilized relative to the combination of two constituent single-quantum states.

By comparing the Δ values of different dye molecules, we can get a glimpse of the effect of molecular geometry on the correlations among the excitations. As shown in the caption of Figure 7, Δ changes sensitively with chemical structure of the molecules. In particular, there is a surprising variation among dye molecules of similar structures. For
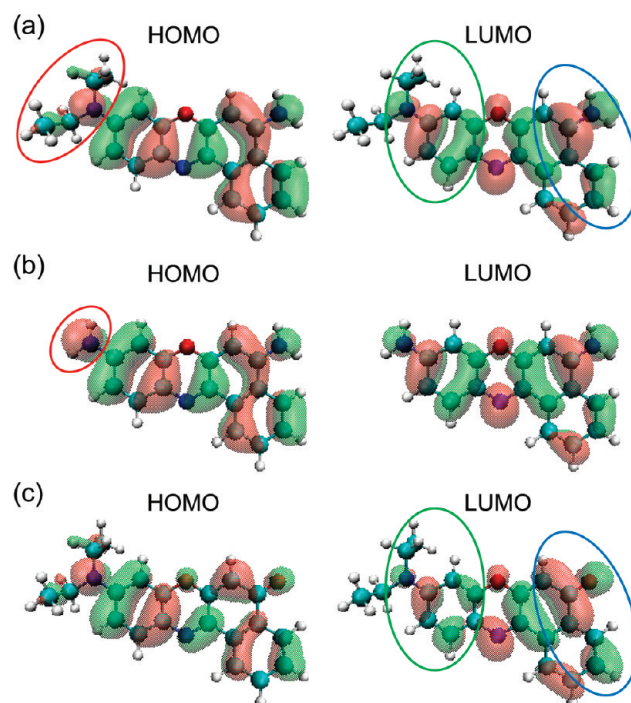

FIGURE 8. Frontier molecular orbitals of (a) NB, (b) CV, and (c) Phen9 plotted with a common surface threshold. At the left end of the molecule, NB has a diethyl amino group, -N(CH$_2$CH$_3$)$_2$, which is more electron-rich than an amino group, -NH$_2$, at the same site of CV, resulting in higher electron density in NB than in CV (compare red circles). In contrast, at the upper right end of the molecule, Phen9 has a carbonyl group, C=O, which is a more electron-withdrawing group than an iminium group, C=NH$_2^+$, at the same site of NB. As a result, a portion of electron density is shifted from one region (green circle) to another (blue circle) in Phen9 compared with that in NB.

example, NB, CV, and Phen9 have a common structural motif with a heterocyclic structure consisting of four rings at their core, while they differ only in their substituent functional groups (see Figure 6). In contrast to the weakly interacting electron model (e.g., as used in band theory of semiconductors), the functional groups on the chromophore have a significant influence on the double-quantum correlation energy. However, these substituents do have a significant effect on the mean-field properties of these molecules, such as the frontier molecular orbitals and electronic transition energies computed at the CI-singles level. The frontier molecular orbitals of NB, CV, and Phen9 were calculated (Hartree–Fock, 6-31G(d) basis set) and are shown in Figure 8. It can be clearly seen that the way the molecular orbitals are delocalized depends on the substituent functional groups, and this in turn will affect the double-quantum correlation energy. Note that a challenge for conceptualizing electron correlation is that it is not directly represented in these orbital pictures (the Hartree–Fock method is a mean-field approach).

5. Conclusions and Outlook

In this Account, it was demonstrated that 2D-DQCS maps out the energies and wave functions of double-quantum states in terms of constituent single-quantum states. In particular, the energies of and correlations among single- and double-quantum states are directly spanned in a two-dimensional frequency space with narrow peak widths in the antidiagonal direction, allowing the achievement of higher spectral resolution than would be obtained by traditional linear and two-photon absorption spectroscopies. The variation of the double-quantum correlation energy, Δ, with molecular geometry suggests that 2D-DQCS provides a sensitive means of probing subtle effects of correlations among the electrons and excitations on the electronic structure. Thus, the 2D-DQCS technique is envisioned to be effective for revealing the electronic structure of highly excited states with double-quantum character even in complex systems. In particular, the full potential of the 2D-DQCS will be fulfilled when it is applied to systems with multiple excited states, for example, excitonic systems, rather than simple three-level systems investigated in this work. For example, anharmonicity of the electronic oscillators studied in this work can be also obtained by 2D-PE, which makes use of only single-quantum coherences. However, when multiple excited states are present, it becomes hard to analyze the resultant complicated peak patterns of 2D-PE spectra containing both single- and double-quantum coherence features. In contrast, the 2D-DQC spectra can directly map out the correlations between double excited and their constituent single excited states in the two different frequency axes.

This spectroscopy provides quantitative insight into highly excited states of molecules in the condensed phase. Calculating these states accurately is one of the greatest challenges for quantum chemistry, and the availability of this experimental probe may stimulate further progress in that field. A challenge lies in interpreting the meaning of the correlation shift Δ and, in turn, working out how to use it as a probe of molecular structure or even chemical reactions. A challenge from an experimental viewpoint is to map out more of frequency space, using shorter pulses or perhaps two-color approaches, because clearly more information can be obtained by expanding the spectral range of the 2D data.

BIOGRAPHICAL INFORMATION

Jeongho Kim received his B.S. degree in chemistry from Korea Advanced Institute of Science and Technology. Then, he earned his M.S. and Ph.D. degrees in chemistry from the University of Chicago under the advisement of Prof. Norbert Scherer. Upon graduating in 2004, he moved to the University of Toronto as a postdoctoral fellow under Prof. Gregory Scholes. His major research interests are to investigate the fast dynamics in the excited electronic states of molecular systems and nanoscale materials using ultrafast nonlinear spectroscopy.

Shaul Mukamel, currently the Chancellor Professor of Chemistry at the University of California, Irvine, received his Ph.D. in 1976 from Tel Aviv University and has held faculty positions at Rice University, the Weizmann Institute, and the University of Rochester. He is the recipient of the Sloan, Dreyfus, Guggenheim, the Alexander von Humboldt Senior Scientist award, and the Lippincort Award and is a fellow of the American Physical society and the Optical Society of America. His interests focus on the theory of ultrafast nonlinear spectroscopy of molecules and semiconductor nanostructures, attosecond X-ray spectroscopy, many-body effects in quantum optics, and nonequilibrium fluctuations in open systems. He is the author of the textbook *Principles of Nonlinear Optical Spectroscopy*.

Gregory Scholes is an Associate Professor at the University of Toronto in the Department of Chemistry. He obtained B.Sc. (Hons.) (1990) and Ph.D. (1994) degrees from the University of Melbourne, then undertook postdoctoral studies at Imperial College in London as a Ramsay Memorial Research Fellow and at the University of California, Berkeley. He is presently an NSERC E.W.R. Steacie Fellow. His present research focuses on elucidating the principles deciding electronic structure, optical properties, and reactions of nanoscale systems by combining synthesis, theory, and ultrafast laser spectroscopy.

REFERENCES

1 Hamm, P.; Lim, M.; Hochstrasser, R. M. Structure of the amide I band of peptides measured by femtosecond nonlinear-infrared spectroscopy. *J. Phys. Chem. B* **1998**, *102*, 6123–6138.

2 Asplund, M. C.; Zanni, M. T.; Hochstrasser, R. M. Two-dimensional infrared spectroscopy of peptides by phase-controlled femtosecond vibrational photon echoes. *Proc. Natl. Acad. Sci. U.S.A.* **2000**, *97*, 8219–8224.

3 Golonzka, O.; Khalil, M.; Demirdoven, N.; Tokmakoff, A. Vibrational anharmonicities revealed by coherent two-dimensional infrared spectroscopy. *Phys. Rev. Lett.* **2001**, *86*, 2154–2157.

4 Zheng, J.; Kwak, K.; Asbury, J.; Chen, X.; Piletic, I. R.; Fayer, M. D. Ultrafast dynamics of solute-solvent complexation observed at thermal equilibrium in real time. *Science* **2005**, *309*, 1338–1343.

5 Mukamel, S. Multidimensional femtosecond correlation spectroscopies of electronic and vibrational excitations. *Annu. Rev. Phys. Chem.* **2000**, *51*, 691–729.

6 Hybl, J. D.; Ferro, A. A.; Jonas, D. M. Two-dimensional Fourier transform electronic spectroscopy. *J. Chem. Phys.* **2001**, *115*, 6606–6622.

7 Brixner, T.; Mancal, T.; Stiopkin, I. V.; Fleming, G. R. Phase-stabilized two-dimensional electronic spectroscopy. *J. Chem. Phys.* **2004**, *121*, 4221–4236.

8 Cho, M. Coherent two-dimensional optical spectroscopy. *Chem. Rev.* **2008**, *108*, 1331–1418.

9 Mukamel, S.; Tortschanoff, A. Multiple quantum coherences in liquid state NMR and nonlinear optics: Collective vs local origin. *Chem. Phys. Lett.* **2002**, *357*, 327–335.

10 Mukamel, S.; Oszwaldowski, R.; Yang, L. A coherent nonlinear optical signal induced by electron correlations. *J. Chem. Phys.* **2007**, *127*, 221105.

11 Abramavicius, D.; Voronine, D. V.; Mukamel, S. Double-quantum resonances and exciton-scattering in coherent 2D spectroscopy of photosynthetic complexes. *Proc. Natl. Acad. Sci. U.S.A.* **2008**, *105*, 8525–8530.

12 Fulmer, E. C.; Mukherjee, P.; Krummel, A. T.; Zanni, M. T. A pulse sequence for directly measuring the anharmonicities of coupled vibrations: Two-quantum two-dimensional infrared spectroscopy. *J. Chem. Phys.* **2004**, *120*, 8067–8078.

13 Warren, W. S.; Huang, S. Y.; Ahn, S.; Lin, Y. Y. Understanding third-order dipolar effects in solution nuclear magnetic resonance: Hahn echo decays and intermolecular triple-quantum coherences. *J. Chem. Phys.* **2002**, *116*, 2075–2084.

14 Li, X.; Zhang, T.; Borca, C. N.; Cundiff, S. T. Many-body interactions in semiconductor probed by optical two-dimensional Fourier transform spectroscopy. *Phys. Rev. Lett.* **2006**, *96*, 057406.

15 Gundogdu, K.; Stone, K. W.; Turner, D. B.; Nelson, K. A. Multidimensional coherent spectroscopy made easy. *Chem. Phys.* **2007**, *341*, 89–94.

16 Scholes, G. D.; Rumbles, G. Excitons in nanoscale systems. *Nat. Mater.* **2006**, *5*, 683–696.

17 Wilson, S. *Electron Correlation in Molecules*; Oxford University Press: Oxford, U.K., 1984; p 292.

18 March, N. H., *Electron Correlation in Molecules and Condensed Phases*. Plenum Press: New York, 1996; p 440.

19 Raghavachari, K. Electron correlation techniques in quantum chemistry: Recent advances. *Annu. Rev. Phys. Chem.* **1991**, *42*, 615–642.

20 Raghavachari, K.; Anderson, J. B. Electron correlation effects in molecules. *J. Phys. Chem.* **1996**, *100*, 12960–12973.

21 Dreuw, A.; Head-Gordon, M. Single-reference ab initio methods for the calculation of excited states of large molecules. *Chem. Rev.* **2005**, *105*, 4009–4037.

22 Starcke, J. H.; Wormit, M.; Schirmer, J.; Dreuw, A. How much double excitation character do the lowest excited states of linear polyenes have? *Chem. Phys.* **2006**, *329*, 39–49.

23 Li, Z.; Abramavicius, D.; Mukamel, S. Probing electron correlations in molecules by two-dimensional coherent optical spectroscopy. *J. Am. Chem. Soc.* **2008**, *130*, 3509–3515.

24 Mukamel, S.; Abramavicius, D.; Yang, L.; Zhuang, W.; Schweigert, I. V.; Voronine, D. V. Coherent multidimensional optical probes for electron correlations and exciton dynamics from NMR to X-rays. *Acc. Chem. Res.* **2009**, *42*, 553–562.

25 Efros, A. L.; Rosen, M.; Kuno, M.; Nirmal, M.; Norris, D. J.; Bawendi, M. Band-edge exciton in quantum dots of semiconductors with a degenerate valence band: Dark and bright exciton states. *Phys. Rev. B* **1996**, *54*, 4843–4856.

26 Scholes, G. D. Controlling the optical properties of inorganic nanoparticles. *Adv. Funct. Mater.* **2008**, *18*, 1157–1172.

27 Wong, C. Y.; Kim, J.; Nair, P. S.; Nagy, M. C.; Scholes, G. D. Relaxation in the exciton fine structure of semiconductor nanocrystals. *J. Phys. Chem. C* **2009**, *113*, 795–811.

28 Salvador, M. R.; Nair, P. S.; Cho, M.; Scholes, G. D. Interaction between excitons determines the non-linear response of nanocrystals. *Chem. Phys.* **2008**, *350*, 56–68.

29 Zahlan, A. B. *The Triplet State*; Cambridge University Press: New York, 1967.

30 Hudson, B. S.; Kohler, B. E. Linear polyene electronic structure and spectroscopy. *Annu. Rev. Phys. Chem.* **1974**, *25*, 437–460.

31 Orlandi, G.; Zerbetto, F.; Zgierski, M. Z. Theoretical analysis of spectra of short polyenes. *Chem. Rev.* **1991**, *91*, 867–891.

32 Yaron, D.; Silbey, R. Effects of electron correlation on the nonlinear optical properties of polyacetylene. *Phys. Rev. B* **1992**, *45*, 11655–11666.

33 Brédas, J. L.; Beljonne, D.; Coropceanu, V.; Cornil, J. Charge-transfer and energy-transfer processes in p-conjugated oligomers and polymers: A molecular picture. *Chem. Rev.* **2004**, *104*, 4971–5004.

34 Abramavicius, D.; Palmieri, B.; Voronine, D. V.; Šanda, F.; Mukamel, S. Coherent multidimensional optical spectroscopy of excitons in molecular aggregates: Quasiparticle versus supermolecule perspectives. *Chem. Rev.* **2009**, *109*, 2350–2408.

35 Salvador, M. R.; Hines, M. A.; Scholes, G. D. Exciton-bath coupling and inhomogeneous broadening in the optical spectroscopy of semiconductor quantum dots. *J. Chem. Phys.* **2003**, *118*, 9380–9388.

36 Collini, E.; Scholes, G. D. Coherent intrachain energy migration in a conjugated polymer at room temperature. *Science* **2009**, *323*, 369–373.

37 Hybl, J. D.; Christophe, Y.; Jonas, D. M. Peak shapes in femtosecond 2D correlation spectroscopy. *Chem. Phys.* **2001**, *266*, 295–309.

38 Yetzbacher, M. K.; Belabas, N.; Kitney, K. A.; Jonas, D. M. Propagation, beam geometry, and detection distortions of peak shapes in two-dimensional Fourier transform spectra. *J. Chem. Phys.* **2007**, *126*, 044511.